

A STUDY OF DYNAMIC HYSTERESIS MODEL FOR A MAGNETORHEOLOGICAL DAMPER

KUN-YUNG CHEN

Department of Aircraft Engineering, Air Force Institute of Technology, Taiwan R.O.C.
e-mail: 9615906@nkust.edu.tw

MING-LUNG KUNG

Department of Avionics Engineering, Air Force Academy, Taiwan R.O.C.
e-mail: d993010015@nsysu.edu.tw

The paper proposes a new dynamic model based on the LuGre model and an electrical equation to describe the hysteresis phenomenon for a magnetorheological (MR) damper. In addition, a sliding mode observer (SMO) is proposed to estimate unmeasurable states of the MR damper. The parameters of the MR damper are successfully identified by using the self-learning particle swarm optimization (SLPSO) algorithm. The contributions of this paper are: i) a new dynamic model based on the LuGre model and an electrical equation for an MR damper is successfully formulated to fit for the hysteresis behavior, ii) the exerted damping force can be practically adjusted by using input voltage for the dynamic model, iii) the SMO is proposed to estimate the internal states and current, and iv) the unknown parameters of the MR damper are successfully identified by using the SLPSO algorithm with a numerical experiment.

Keywords: identification, LuGre model, magnetorheological damper, self-learning particle swarm optimization (SLPSO), sliding mode observer (SMO)

1. Introduction

The magnetorheological (MR) damper is a well known semi-active shock absorber which has been extensively studied and investigated recently. Characteristics of MR dampers include low power requirements, simple construction, quick response and adjustable damping force. Currently, they are widely applied in vehicle suspension systems and civil engineering to absorb shocks. However, the nonlinear hysteresis phenomenon of MR dampers is an inherent and complicated problem. Accordingly, how to correctly describe the hysteresis phenomenon with a simple dynamic model for the MR damper is a significant and interesting research area. Previously, the Bouc-Wen model has been widely implemented to characterize the hysteresis phenomenon (Ismail *et al.*, 2009; Ikhoulane and Rodellar, 2005, 2007; Metered, 2010; Bhowmik, 2011; Ambhore *et al.*, 2013). Moreover, the development of the Bouc-Wen model to describe the hysteresis phenomenon in dynamically excited nonlinear structures has been reviewed (Ismail *et al.*, 2009). Moreover, standard and modified Bouc-Wen models have been proposed in the literature (Ikhoulane and Rodellar, 2005; Metered, 2010; Bhowmik, 2011; Ambhore *et al.*, 2013). Recently, Ramli *et al.* (2019) proposed a Bouc-Wen model to describe the dynamic behavior of smart material-based actuators, then designed an adaptive controller to implement in a smart actuator. In (Naz *et al.*, 2021), a piezo-stage actuator that was modelled based on the nonlinear Bouc-Wen hysteresis model was numerically studied and presented. The performance of the positioning system model was validated through accuracy measurements and a regression analysis.

In (Balamurugan and Jancirani, 2013), a modified parametric algebraic model was presented that was able to control a semi-active suspension system, and the effectiveness and robustness of

the semi-active control approach was demonstrated in simulations. To investigate the dynamics of a damper filled with an MR fluid, a lumped mass thermo-mechanical model was proposed and studied in (Zalewski *et al.*, 2014). Several effects (including friction and temperature) were discussed in this model and the piston displacement coupled with the energy balance equation for temperature was analyzed. In (Boada *et al.*, 2018), an inverse MR damper model based on network inversion was proved in experimental tests to estimate the input current and voltage, and the damping force was exerted by an MR damper. In (Graczykowski and Pawłowski, 2017), the damper response of an MR fluid was modeled using thermodynamic equations which described reduced and parametric models in terms of relative phenomena. Recently, a generalized hysteretic bi-viscous operator was proposed in (Zhao *et al.*, 2018) for approximate description of hysteretic properties. In the aforementioned studies, different types of mathematical models were proposed to properly characterize the nonlinear hysteresis phenomenon in the input current. However, it is impractical to adjust the damping force using the input current for an MR damper. Therefore, a mathematical model using the input voltage is more practical for adjusting the damping force.

Determination of the unknown parameters in the proposed dynamic model is a significant task. Here, the parameter identification method is suitable for finding the unknown parameters of the dynamic model. Recently, some studies about parameter identification for MR dampers have been conducted. For example, parameter identification in typical loading cases was studied in (Peng *et al.*, 2018), and the authors established a functional relationship with the input current. Moreover, these parameters were defined and optimized by a genetic algorithm integrated with the Simulink toolbox in MATLAB. In (Pellicciari *et al.*, 2018), a pinched hysteretic system was modelled using a modified Bouc-Wen model. There, parameter identification for the hysteretic system was performed by using a genetic algorithm, and the numerical results were successful. A normalized Bouc-Wen model was employed in (Zhu *et al.*, 2019) to describe the hysteresis of an MR damper. Then, a genetic algorithm was utilized to identify the parameters of the MR damper, and the simulation results indicated that the proposed method was more accurate. A constrained unscented Kalman filter was proposed in (Niola *et al.*, 2019) to identify the parameters of the hysteresis model. There, the Bouc-Wen model was adopted to describe the hysteretic behavior for a seismic isolator. The results indicated that the proposed Kalman filter provided an improved parameter identification ability. A modified Bouc-Wen hysteresis model was adopted in (Bartkowski *et al.*, 2019) to describe nonlinear responses of tested specimens, and a genetic algorithm was applied to identify the model parameters. In (Nguyen *et al.*, 2022), a novel adaptive parameter identification method was proposed for a model consisting of an estimated model, a hysteresis observer, and adaptive algorithms. The mentioned models, including the Bouc-Wen one, LuGre and Dahl friction model for MR dampers, still have many unknown parameters to find to fit the real dampers. System parameter identification is a practical method that uses intelligence algorithms, including the particle swarm optimization algorithm, dynamic neural networks and genetic algorithms. If a fitness function (FF) is defined with an error function between the real and estimated damping force, these algorithms can randomly search for proper parameters to optimize (maximize or minimize) the FF, and these proper parameters are the final solutions.

In this paper, a modified LuGre friction model (Jiménez and Álvarez-Icaza, 2005) is implemented to characterize the nonlinear hysteresis phenomenon for an MR damper. The control input voltage can change the current to adjust the damping force. However, the control input voltage is more practical than the control input current for MR dampers during real operation. Therefore, an electrical equation including resistance, inductance and induced electromotive force is considered and integrated into the dynamic model. In other words, a new dynamic model with an electrical equation for MR dampers is formulated and presented in this paper. In addition, a sliding mode observer (SMO) is proposed to estimate unmeasurable states of the MR damper. Then, the self-learning particle swarm optimization (SLPSO) (Li *et al.*, 2012) is

proposed to identify the unknown parameters. An FF is defined as the absolute error between the real and estimated damping force. Three types of input voltage are implemented to verify the efficiency of the parameter identification, where it is revealed that a varying input voltage can excite more varying output responses, which are used to correctly identify the unknown parameters. From the simulation results, the new dynamic model was successfully formulated. The proposed identification method is practicable for dynamic modelling of an MR damper to identify the unknown parameters.

Finally, the remainder of this paper is organized as follows: Section 1 presents the introduction, Section 2 contains dynamic modeling of an MR damper, Section 3 presents parameter identification, whereas numerical experiments and conclusions are described in Sections 4 and 5, respectively.

2. Dynamic modeling

An MR damper is a shock absorber filled with a magnetorheological fluid, and the exerted damping force can be adjusted by the magnetic field via the input current. The damping characteristic of an MR damper can be continuously adjusted by changing the power of the electromagnet, whereby the fluid viscosity increases within the damper as the electromagnetic intensity increases. In traditional dampers, the relationship between the damping force f_d and velocity v is linear, which can be represented as $f_d = \mu v$, where μ is the damping coefficient. However, the relation of the damping force with input velocity and displacement for the MR damper is a nonlinear hysteresis phenomenon. Therefore, formulating an appropriate dynamic model of the MR damper that completely describes the hysteresis behavior is a significant challenge.

2.1. Mathematical model based on the LuGre model

In this study, one can find a dynamic model to describe the hysteresis phenomenon of the MR damper. The hysteresis phenomenon can also be found in various fields, including physics, chemistry, engineering, biology and economics. Moreover, previous models, such as the Preisach (Roussel *et al.*, 2022a,b) and Duhem models (Ahmed *et al.*, 2021; Xu *et al.*, 2022) have been proposed to describe nonlinear hysteresis systems. Many dynamic models have also been developed to describe such hysteresis behavior, and it is necessary to select and implement high-accuracy models to capture nonlinear hysteretic responses. For example, traditional and modified Bouc-Wen models (Ramli *et al.*, 2019; Naz *et al.*, 2021; Peng *et al.*, 2018; Pellicciari *et al.*, 2019) have been proposed to describe hysteretic responses of an MR damper. The Bouc-Wen model comprises three parts (spring, damper and Bouc-Wen block) and includes an evolutionary variable, internal displacement and external excitation displacement. However, the evolutionary variable and internal displacement are unmeasurable, which is a disadvantage in practical operations. A diagram of an MR damper is presented in Fig. 1, where I is the input current and terms x and v are the external excitation displacement and velocity, respectively. In this paper, the LuGre mathematical model (Jiménez and Álvarez-Icaza, 2005) has been adopted to describe the hysteretic behavior, which is written as follows

$$\dot{z} = v - \alpha|v|z \quad f = \beta(I)v + \delta x + \varepsilon\dot{z} + \gamma(I)z + f_0 \quad (2.1)$$

where z is the internal state variable, f is the damping force exerted by the MR damper, α , δ and ε are the positive constants, and f_0 is the known damping force. The functions $\beta(I)$ and $\gamma(I)$ with the input current I are written as follows

$$\beta(I) = -p_1 I^2 + p_2 I + p_3 \quad \gamma(I) = q_1 I + q_2 \quad (2.2)$$

where $p_{1,2,3}$ and $q_{1,2}$ are the positive constants. The mathematical model using the LuGre model of the MR damper is proposed in Eqs. (2.1). It is evident that the internal state of z is the only unknown variable in the mathematical model, which can be estimated by a state observer.

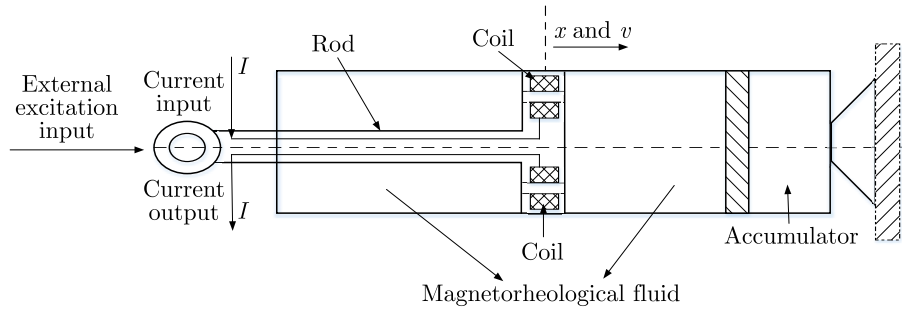


Fig. 1. A diagram of an MR damper

2.2. Electrical equation

Although the input current I is produced by the input voltage, it is easier to change the exerted damping force by adjusting the input voltage in practical applications of the MR damper. Then, an electrical equation that includes the control input voltage, resistance and inductance is necessary when formulating the dynamic model. The resistor-inductor circuit is the general electrical circuit that is suitable for the MR damper model. In particular, the induced electromotive force (EMF) that occurs between the coil and MR fluid is considered in the dynamic model. According to Faraday's law, the EMF \mathcal{J} is formally defined as

$$\mathcal{J} = N \frac{d\Phi_B}{dt} \quad (2.3)$$

where \mathcal{J} is the EMF, N is the number of turns on the coil, and Φ_B is the magnetic flux. It is known that MR fluids are filled with micrometer-sized magnetizable particles. When the magnetic field induced by the current in the coil and the magnetizable particles pass through the coil, the magnetic flux is directly proportional to the velocity of the magnetizable particles. According to this description, the following expression can be obtained

$$\mathcal{J} = \lambda v \quad (2.4)$$

where λ is the EMF constant. Therefore, the completed electrical equation that includes the input voltage, resistance, inductance and EMF is as follows

$$U = IR + L \frac{dI}{dt} + \lambda v \quad (2.5)$$

where U is the input voltage, R is the resistance, and L is the inductance. The electrical parameters R , L and λ are assumed constant without any temperature effect. The mathematical model with the LuGre model for the MR damper is proposed in Eqs. (2.1). In addition, the complete electrical equation is formulated in Eq. (2.5). To integrate the exerted damping force with the electrical equation, a diagram of an operational MR damper is presented in Fig. 2. When the external excitation displacement x and velocity v are applied to the MR damper, the exerted damping force f is produced, which can be adjusted with the input current I . Then, the damping force can be measured by using a load cell transferred to a personal computer (PC). Here, the PC receives signals including the damping force, external excitation displacement and velocity. Accordingly, the diagram of the MR damper is successfully designed, which can be extensively implemented in the system modeling, parameter identification and vibration control.

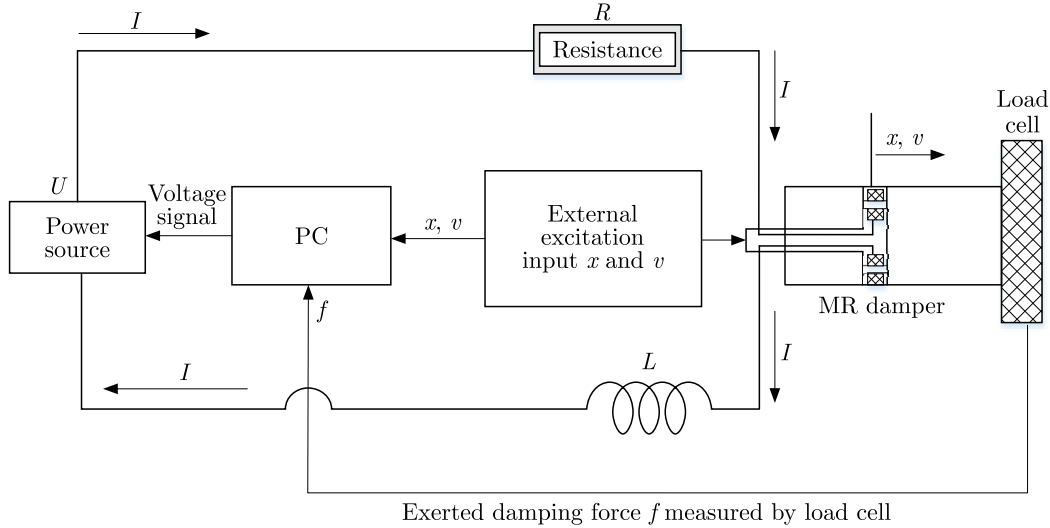


Fig. 2. A diagram of an operational MR damper

Finally, the proposed dynamic model with a state-space matrix form using Eqs. (2.1)₁ and (2.5) can be formulated as

$$\dot{\mathbf{X}} = \mathbf{A}\mathbf{X} + \mathbf{B}\mathbf{W} \quad \mathbf{Y} = \mathbf{C}\mathbf{X} \tag{2.6}$$

where

$$\mathbf{X} = \begin{bmatrix} x \\ z \\ I \end{bmatrix} \quad \mathbf{A} = \begin{bmatrix} 0 & 0 & 0 \\ 0 & -\alpha|v| & 0 \\ 0 & 0 & \frac{-R}{L} \end{bmatrix} \quad \mathbf{B} = \begin{bmatrix} 1 & 0 & 0 \\ 0 & 1 & 0 \\ 0 & \frac{-\lambda}{L} & \frac{1}{L} \end{bmatrix}$$

$$\mathbf{W} = [v, v, U]^T \quad \mathbf{C} = [1, 0, 0]$$

In particular, \mathbf{X} is the system state vector, \mathbf{Y} is the system output, \mathbf{A} and \mathbf{B} are the system matrices, \mathbf{W} is the input vector, and terms v and U are the inputs.

3. Parameter identification

Dynamic modeling of a system is the first step toward analyzing an engineering problem. In Section 2, the dynamic model of an MR damper is formulated by Eqs. (2.6). The exerted damping force for an MR damper is also included in Eq. (2.1)₂. Moreover, there are 11 unknown parameters ($\alpha, \delta, \varepsilon, p_{1,2,3}, q_{1,2}, R, L$ and λ) in the dynamic model using Eqs. (2.1)₂ and (2.6). In this study, parameter identification is proposed to identify these unknown parameters. First, the SLPSO algorithm (Li *et al.*, 2012) is employed to find the unknown parameters. Then, the FF can be defined as an object function to be optimized by the SLPSO algorithm. When the SLPSO algorithm has optimized the FF with a set of parameters, the final parameters are the solutions for the unknown parameters.

3.1. Self-learning particle swarm optimization

Although the conventional PSO algorithm can find the local optimal solution to an optimization problem, the method is awkward when dealing with a complex and nonlinear optimization problem. Therefore, the SLPSO algorithm has been developed to deal with nonlinear systems and global optimization problems. The SLPSO has advantages including global optimization,

rapid convergence and searching ability, which are suitable for performing system parameter identification for the MR damper. First, the basic updated equation for the standard PSO for each particle j is described as follows

$$x_j'^d = x_j^d + v_j'^d \quad (3.1)$$

where $x_j'^d$ and x_j^d represent the current and previous positions in the d -th dimension for the particle j , respectively, while $v_j'^d$ is the current velocity. For the standard PSO algorithm, the updated equation of the particle velocity is as follows

$$v_j'^d = wv_j^d + \eta_1 r_1 (x_{pbest_j}^d - x_j^d) + \eta_2 r_2 (x_{gbest}^d - x_j^d) \quad (3.2)$$

where $w \in (0, 1)$ is the inertia weight, v_j^d is the previous velocity for the particle j , η_1 and η_2 are positive acceleration constants, r_1 and r_2 are random numbers from 0 to 1, $x_{pbest_j}^d$ is the best position found for the particle j so far, and x_{gbest}^d is the best position found by the whole set of particles so far. When the current velocity $v_j'^d$ is updated, the new position $x_j'^d$ is updated to minimize the objective function for each iteration. However, the SLPSO has four velocity-updated strategies (exploitation, jumping out, exploration and convergence) to enable each particle to independently deal with different situations. For each particle j , the learning equations corresponding to the four operators are respectively given as follows:

1) Operator a: learning from its $pbest$ position

$$\text{exploitation: } v_j'^d = wv_j^d + \eta_3 r_j^d (pbest_j^d - x_j^d) \quad (3.3)$$

2) Operator b: learning from a random position nearby

$$\text{jumping out: } x_j'^d = x_j^d + v_a v_{avg}^d N(0, 1) \quad (3.4)$$

3) Operator c: learning from the $pbest$ of a random particle

$$\text{exploration: } v_j'^d = wv_j^d + \eta_3 r_j^d (pbest_{rand}^d - x_j^d) \quad (3.5)$$

4) Operator d: learning from the $abest$ position

$$\text{convergence: } v_j'^d = wv_j^d + \eta_3 r_j^d (abest^d - x_j^d) \quad (3.6)$$

where r_j^d is the random number for each particle j , η_3 is the acceleration constant, and $pbest_{rand}^d$ is the $pbest$ of a random particle (which is better than $pbest_j$). The jumping step $v_a v_{avg}^d$ is the average speed of all particles in the d -th dimension, which is calculated using $v_{avg}^d = \sum_{j=1}^N |v_j^d|/N$, and N is the population size, where $N(0, 1)$ is a random number generated from the normal distribution with a mean of 0 and a variance of 1. The $abest$ position is an archive of the best position found so far. Finally, the position of each particle is updated to minimize the objective function.

In the SLPSO algorithm, each particle has its own velocity-updating strategy to address different situations for a nonlinear system. The cooperation of the four strategies is implemented by an adaptive learning framework at an individual level, which enables each particle to choose an optimal strategy according to its own local fitness landscape. The performing procedure for the SLPSO algorithm can be found in (Li *et al.*, 2012).

3.2. Sliding mode observer

For the dynamic model with the LuGre model in Eq. (2.1)₁, the variable z is an internal state and is unmeasurable. In addition, the current I is unknown. To solve the problem of estimating the states of z and I , a state observer can be implemented. The conditions are that the external excitation displacement x , velocity v and the input voltage U are known. Moreover, the system matrices \mathbf{A} and \mathbf{B} and the input vector \mathbf{W} in Eq. (2.6)₁ are also known. The unknown states of z and I must be rapidly estimated to converge toward the real states. Therefore, a sliding mode observer (SMO) in accordance with Eq. (2.6)₁ is written as follows

$$\dot{\hat{\mathbf{X}}} = \mathbf{A}\hat{\mathbf{X}} + \mathbf{B}\mathbf{W} + \Delta \quad (3.7)$$

where $\hat{\mathbf{X}} = [\hat{x}, \hat{z}, \hat{I}]^T$, $\Delta = \mathbf{K}\varepsilon$, $\mathbf{K} = [k_1, k_2, k_3]^T$, $\varepsilon = |e| \operatorname{sgn}(e)$, and $e = \hat{x} - x$, \hat{x} , \hat{z} and \hat{I} are the estimated displacement, internal state and current, respectively. Terms k_1 , k_2 and k_3 are known positive constants. The corresponding error dynamic equation between Eqs. (2.6)₁ and (3.7) is

$$\dot{\mathbf{E}} = \mathbf{A}\mathbf{E} + \Delta \quad (3.8)$$

where $\mathbf{E} = \hat{\mathbf{X}} - \mathbf{X} = [\hat{x} - x, \hat{z} - z, \hat{I} - I]^T$.

If Eq. (3.8) is an asymptotically stable system, then $\mathbf{E} \rightarrow \mathbf{0}$ with $t \rightarrow \infty$ and \mathbf{A} is a stable matrix. Here, the term Δ can be viewed as a control input for the stable system, which should be satisfied as follows

$$\|\Delta\|_2 = \|\mathbf{K}\varepsilon\|_2 \leq \|\mathbf{K}\|_2 \|\varepsilon\|_2 = \|\mathbf{K}\|_2 |e| \leq \gamma \|\mathbf{E}\|_2 \quad (3.9)$$

where $\|\cdot\|_2$ is the Euclidean norm and γ is a positive constant. From the mentioned inequality equation, it is revealed that

$$|e| \leq \|\mathbf{E}\| \quad 0 < \sqrt{k_1^2 + k_2^2 + k_3^2} \leq \gamma \quad (3.10)$$

To prove that the corresponding error dynamic equation is asymptotically stable, a Lyapunov candidate function L can be proposed as follows

$$L = \mathbf{E}^T \mathbf{P} \mathbf{E} \quad (3.11)$$

where $\mathbf{P} \in \mathbb{R}^{3 \times 3}$ is the positive definite and diagonal matrix. The time derivative of L is

$$\dot{L} = \dot{\mathbf{E}}^T \mathbf{P} \mathbf{E} + \mathbf{E}^T \mathbf{P} \dot{\mathbf{E}} = \mathbf{E}^T (\mathbf{A}^T \mathbf{P} + \mathbf{P} \mathbf{A}) \mathbf{E} + 2\mathbf{E}^T \mathbf{P} \Delta \quad (3.12)$$

If the homogeneous system $\dot{\mathbf{E}} = \mathbf{A}\mathbf{E}$ is asymptotically stable, there are positive definite matrices \mathbf{P} and \mathbf{Q} such that

$$\mathbf{A}^T \mathbf{P} + \mathbf{P} \mathbf{A} = -2\mathbf{Q} \quad (3.13)$$

where $\mathbf{Q} \in \mathbb{R}^{3 \times 3}$ is the positive definite matrix. Then, Eq. (3.12) can be obtained as

$$\dot{L} = -2(\mathbf{E}^T \mathbf{Q} \mathbf{E} - \mathbf{E}^T \mathbf{P} \Delta) \quad (3.14)$$

According to the Rayleigh principle (Andersen, 2000)

$$\lambda_{\max}(\mathbf{Q}) \mathbf{E}^T \mathbf{E} \geq \mathbf{E}^T \mathbf{Q} \mathbf{E} \geq \lambda_{\min}(\mathbf{Q}) \mathbf{E}^T \mathbf{E} = \lambda_{\min}(\mathbf{Q}) \|\mathbf{E}\|_2^2 \quad (3.15)$$

where λ_{\max} are the maximum eigen values of \mathbf{Q} and λ_{\min} are the minimum eigen values of \mathbf{Q} . Here, inequality equation Eq. (3.9) is used, from which the inequality expression is as follows

$$\mathbf{E}^T \mathbf{P} \Delta \leq \|\mathbf{E}\|_2 \|\mathbf{P}\|_2 \|\Delta\|_2 = \lambda_{\max}(\mathbf{P}) \|\Delta\|_2 \|\mathbf{E}\|_2 \leq \gamma \lambda_{\max}(\mathbf{P}) \|\mathbf{E}\|_2^2 \quad (3.16)$$

where λ_{max} are the maximum eigen values of \mathbf{P} . If the condition satisfies $\mathbf{E}^T \mathbf{Q} \mathbf{E} \geq \mathbf{E}^T \mathbf{P} \mathbf{\Delta}$, then we can find an inequality equation by using Eqs. (3.10)₂, (3.15) and (3.16), as follows

$$0 < \sqrt{k_1^2 + k_2^2 + k_3^2} \leq \gamma \leq \frac{\lambda_{min}}{\lambda_{max}} \quad (3.17)$$

Constants k_1 , k_2 and k_3 can be selected according to the above inequality equations. When the inequality equation $\mathbf{E}^T \mathbf{Q} \mathbf{E} \geq \mathbf{E}^T \mathbf{P} \mathbf{\Delta}$ exists, $\dot{L} \leq 0$ in Eq. (3.14) is obtained as

$$\dot{L} = -2(\mathbf{E}^T \mathbf{Q} \mathbf{E} - \mathbf{E}^T \mathbf{P} \mathbf{\Delta}) \leq 0 \quad (3.18)$$

Then, the error dynamic equation Eq. (3.8) is an asymptotically stable system, and $\mathbf{E} \rightarrow 0$ with $t \rightarrow \infty$. Hence, the proposed SMO can correctly and rapidly estimate the unknown states of z and I to converge toward the real states.

3.3. Parameter identification

In practical applications of MR dampers, the input voltage U , excitation displacement x , excitation velocity v and the output damping force f are known. However, the internal states of z and the current I are unavailable, and the parameters α , δ , ε , p_1 , p_2 , p_3 , q_1 , q_2 , R , L and λ in the dynamic model of the MR damper are also unknown. In the process of identifying these parameters, we can find the identification parameters $\hat{\alpha}$, $\hat{\delta}$, $\hat{\varepsilon}$, \hat{p}_1 , \hat{p}_2 , \hat{p}_3 , \hat{q}_1 , \hat{q}_2 , \hat{R} , \hat{L} and $\hat{\lambda}$. When $\hat{\alpha}$, \hat{R} , \hat{L} and $\hat{\lambda}$ are found, the estimated states of \hat{z} , \hat{z} and \hat{I} can be obtained using the SMO. Then, the identified damping force \hat{f} can be obtained as follows

$$\hat{f} = \hat{\beta}(\hat{I})v + \hat{\delta}x + \hat{\varepsilon}\dot{z} + \hat{\gamma}(\hat{I})\hat{z} + f_0 \quad (3.19)$$

where $\hat{\beta}(\hat{I}) = -\hat{p}_1 \hat{I}^2 + \hat{p}_2 \hat{I} + \hat{p}_3$ and $\hat{\gamma}(\hat{I}) = \hat{q}_1 \hat{I} + \hat{q}_2$.

If the estimated damping force \hat{f} is equal to the real damping force f , we can conclude that the dynamic model is successfully formulated with the identified parameters. Therefore, the FF is proposed as follows

$$\text{FF} = \sum_{i=1}^n |f(t_i) - \hat{f}(t_i)| \quad (3.20)$$

Finally, the process of parameter identification is combined with the SMO. The identified damping force \hat{f} , FF and SLSO algorithms are proposed, and the diagram for parameter identification is displayed in Fig. 3. The real damping force $f(t_i)$ is produced by the external excitation input displacement, velocity and voltage. Then, the SLPSO randomly selects a set of proper parameters $\hat{\alpha}$, $\hat{\delta}$, $\hat{\varepsilon}$, \hat{p}_1 , \hat{p}_2 , \hat{p}_3 , \hat{q}_1 , \hat{q}_2 , \hat{R} , \hat{L} and $\hat{\lambda}$ to minimize the FF at each iteration. When the FF converges toward the minimum value, the final identified parameters are the identification results presented by the SLPSO algorithm.

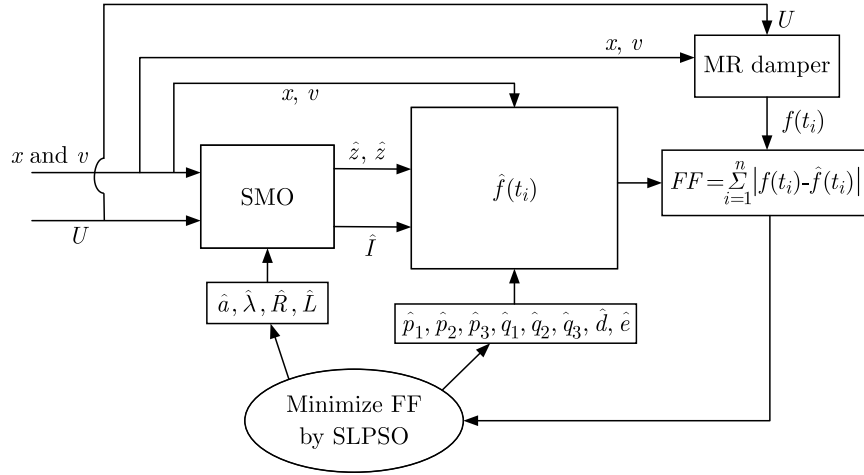
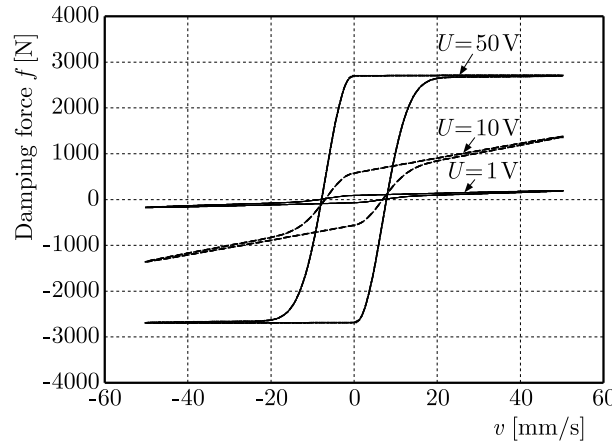
4. Numerical experiments

In the numerical experiments, there are two parts to execute. First, the system state of x of the MR damper is assumed to be available and the SMO is proposed to estimate the unavailable states of z and I . Then, the parameters of the mathematical model are unknown, and the SMO and SLPSO are implemented to identify the unknown parameters. The numerical parameters for numerical experiments are illustrated in Table 1. The dynamic model of the MR damper is solved by the Runge-Kutta method with the ODE 45 function using MATLAB. First, to verify the efficiency of the proposed dynamic model, the external excitation velocity is given as

Table 1. The given numerical parameters for numerical experiments

$\alpha = 3 \text{ mm}^{-1}$, $R = 5$, $L = 0.1 \text{ H}$, $\lambda = 5 \cdot 10^{-5} \text{ Vs/mm}$ $\varepsilon = 0.5 \text{ Ns/mm}$, $\delta = 1 \text{ N/mm}$, $q_1 = 800 \text{ N/A}$, $q_2 = 15 \text{ N}$ $p_1 = 1 \text{ Ns/mmA}^2$, $p_2 = 10 \text{ Ns/mmA}$, $p_3 = 0.5 \text{ Ns/mm}$
--

$v = 16\pi \cos(4\pi/5)t \text{ mm/s}$, and the input voltages are $U = 1 \text{ V}$, $U = 10 \text{ V}$ and $U = 50 \text{ V}$. The phase plane of the damping force versus velocity with different input voltages is shown in Fig. 4, where it is evident that the proposed dynamic model can appropriately describe the hysteresis phenomena for a wide range of the external input velocities, voltages and current.


Fig. 3. Process of parameter identification using the SLPSO algorithm

Fig. 4. Force-velocity plane for the variable input voltages

4.1. Sliding mode observer

To prove the estimation performance of the proposed SMO, the estimated results are demonstrated by using a numerical experiment in this Section. First, when the system matrices \mathbf{A} and \mathbf{B} are known, the input vector \mathbf{W} is given as $v = 12 \cos(\pi t) \text{ mm/s}$ and $U = 10 \sin(\pi t/2) \text{ V}$. Therefore, the real states of z and I can be produced by using the above parameters and input vector in dynamic Eq. (2.6)₁. Nevertheless, for implementation of the SMO, the displacement x is available. The initial conditions of the estimation states are given as $\hat{z}(0) = 1 \text{ mm}$ and $\hat{I}(0) = 2 \text{ A}$.

The constants k_1 , k_2 and k_3 for the SMO are selected according to inequality equations (3.17) to perform the best convergence performance between the real and estimated states. Figure 5 displays the responses between the real and estimated states by using the proposed SMO. A comparison between z and \hat{z} is displayed in Fig. 5a. Although the initial conditions of $z(0)$ and $\hat{z}(0)$ are different, the estimation state of \hat{z} rapidly converges toward the real state of z in the initial period. Similarly, comparisons of I and \hat{I} are displayed in Fig. 5b. Although the initial conditions of $I(0)$ and $\hat{I}(0)$ are different, the estimation state of \hat{I} rapidly converges toward the real state I in the initial period. In summary, the unknown states of z and I can be rapidly and correctly estimated by the SMO proposed in this paper.

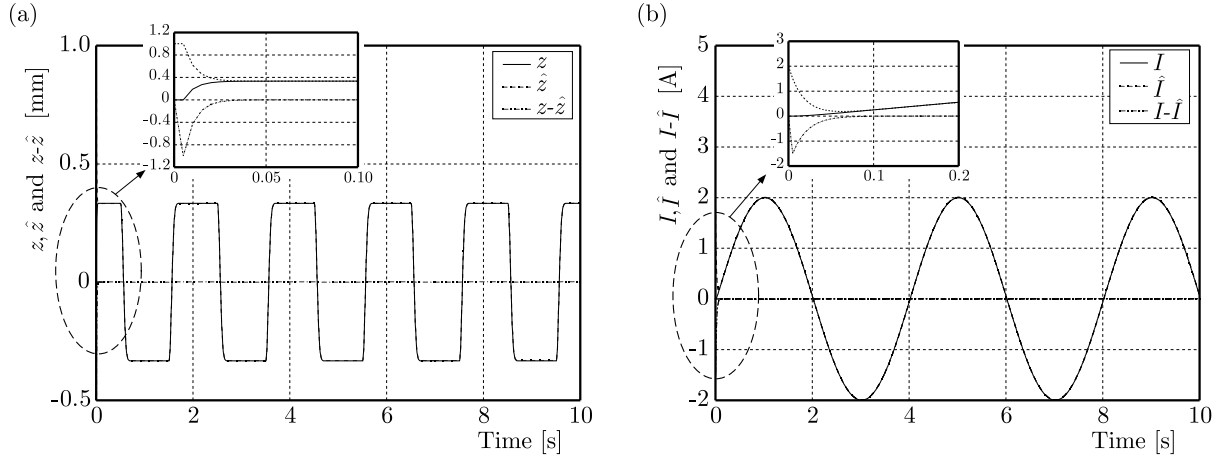


Fig. 5. Responses of the estimated states by using the SMO

4.2. Identification results

The external excitation displacement and velocity are respectively given as $x = 12 \sin(2\pi/2.5)t$ mm and $v = (24\pi/2.5) \cos(2\pi/2.5)t$ mm/s, the operational duration of external excitation is 10s, and the sampling time is $\Delta t = 5 \cdot 10^{-3}$ s. In the numerical experiments, the real exerted damping force f is obtained by using the given parameters, the external excitation displacement and external excitation velocity. However, the adjusting pf the damping force is dependent on the varying input current produced by the input voltage. Therefore, the input voltage plays a major role in producing the damping force. In the process of parameter identification for the MR damper, there are three kinds of input voltages: $U_1 = 10$, $U_2 = |10 \sin(\pi/2.5)t|$ and $U_3 = t$. Accordingly, there are three types of damping forces produced by using U_1 , U_2 and U_3 . The processes of parameter identification using the SLPSO in Fig. 3 are implemented and performed. Table 2 lists the identification results by using U_1 , U_2 and U_3 . The feasible domains for each parameter are given, and the SLPSO algorithm can randomly search for the proper parameters in the feasible domains to minimize the FF. From the identification results, it is evident that the average of absolute error percentage by using U_1 is maximum, and the average absolute error percentage by using U_3 is minimum. A comparison of the responses of the FF by using U_1 , U_2 and U_3 is shown in Fig. 6. Here, it is clear that the responses of the FF by using U_3 is minimum, and the responses of the FF by using U_1 is maximum. From these results, it can be determined that the identified parameters by using U_3 are equivalent to the real parameters. In the numerical experiments, the identified responses of displacement, velocity and damping force are respectively denoted as \hat{x}_1 , \hat{v}_1 and \hat{f}_1 by using the identified parameters with the input voltage U_1 in Table 2. The identified responses of displacement, velocity and damping force are respectively denoted as \hat{x}_2 , \hat{v}_2 and \hat{f}_2 by using the identified parameters by the input voltage U_2 in Table 2. Similarly, the identified responses of displacement, velocity and

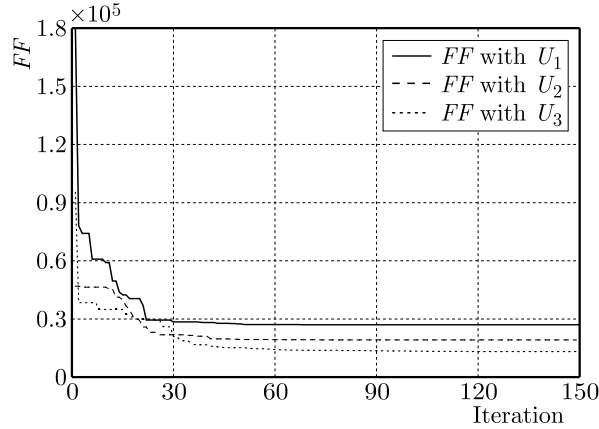


Fig. 6. Responses comparison of FF by using U_1 , U_2 and U_3

Table 2. Identification results by using input voltages U_1 , U_2 and U_3

Parameters	Given values	Feasible domain	Identified values/absolute error percentages		
			U_1	U_2	U_3
α	3	1.5-4.5	2.439/18.69%	2.360/21.31%	2.318/22.71%
R	5	2.5-7.5	7.500/50%	7.500/50%	6.299/25.98%
L	0.1	0.05-0.15	0.141/41%	0.150/50%	0.150/50%
$\lambda(10^{-5})$	5	2.5-7.5	7.500/50%	3.411/31.78%	7.185/43.70%
ε	0.5	0.25-0.75	0.716/43.2%	0.750/50%	0.750/50%
δ	1	0.5-1.5	1.500/50%	1.500/50%	1.500/50%
q_1	800	400-1200	1036.165/29.52%	1054.162/31.77%	869.212/8.65%
q_2	15	7.5-22.5	22.500/50%	18.716/24.77%	9.219/38.54%
p_1	1	0.5-1.5	1.500/50%	1.500/50%	1.215/21.50%
p_2	10	5-15	12.706/27.06%	11.853/18.53%	10.184/1.84%
p_3	0.5	0.25-0.75	0.750/50%	0.494/0.12%	0.750/50%
Average of absolute error percentages [%]			41.77% (Max)	34.39%	32.19% (Min)

damping force are respectively denoted as \hat{x}_3 , \hat{v}_3 and \hat{f}_3 by using the identified parameters by the input voltage U_3 in Table 2. In Fig. 7, the responses of real damping force f are produced with the given parameters ($\alpha, R, L, \dots, p_2, p_3$) in Table 2, whereas the responses of estimated damping forces $\hat{f}_{1,2,3}$ are produced with the identified parameters ($\hat{\alpha}, \hat{R}, \hat{L}, \dots, \hat{p}_2, \hat{p}_3$) by using the input voltages $U_{1,2,3}$, respectively. Comparing the responses of damping forces f and $\hat{f}_{1,2,3}$ versus displacement in Figs. 7a, 7c and 7e, it is evident that the errors between f and \hat{f}_1 are maximum (Fig. 7a), and the errors between f and \hat{f}_3 are minimum (Fig. 7e). Figure 7b displays a comparison of the response between the real damping forces f and \hat{f}_1 versus velocity. Figure 7d presents a comparison between the damping forces f and \hat{f}_2 versus velocity, and Fig. 7f presents a comparison between the damping forces f and \hat{f}_3 versus velocity. Comparing the damping forces between f and $\hat{f}_{1,2,3}$ in Figs. 7b, 7d and 7f, it is clear that the errors between f and \hat{f}_1 are maximum (Fig. 7b), and the errors between f and \hat{f}_3 are minimum (Fig. 7f). From these comparisons, it is evident that the responses of \hat{f}_3 with the identified parameters are similar to the real damping force f .

To confirm the values of the identified parameters in Table 2, the same external excitation displacement and velocity are used, and an other input voltage of $U(t) = 10 \sin(\pi t/10)$, $0 \leq t \leq 10$ s is applied to the MR damper. First, a comparison between the real internal state

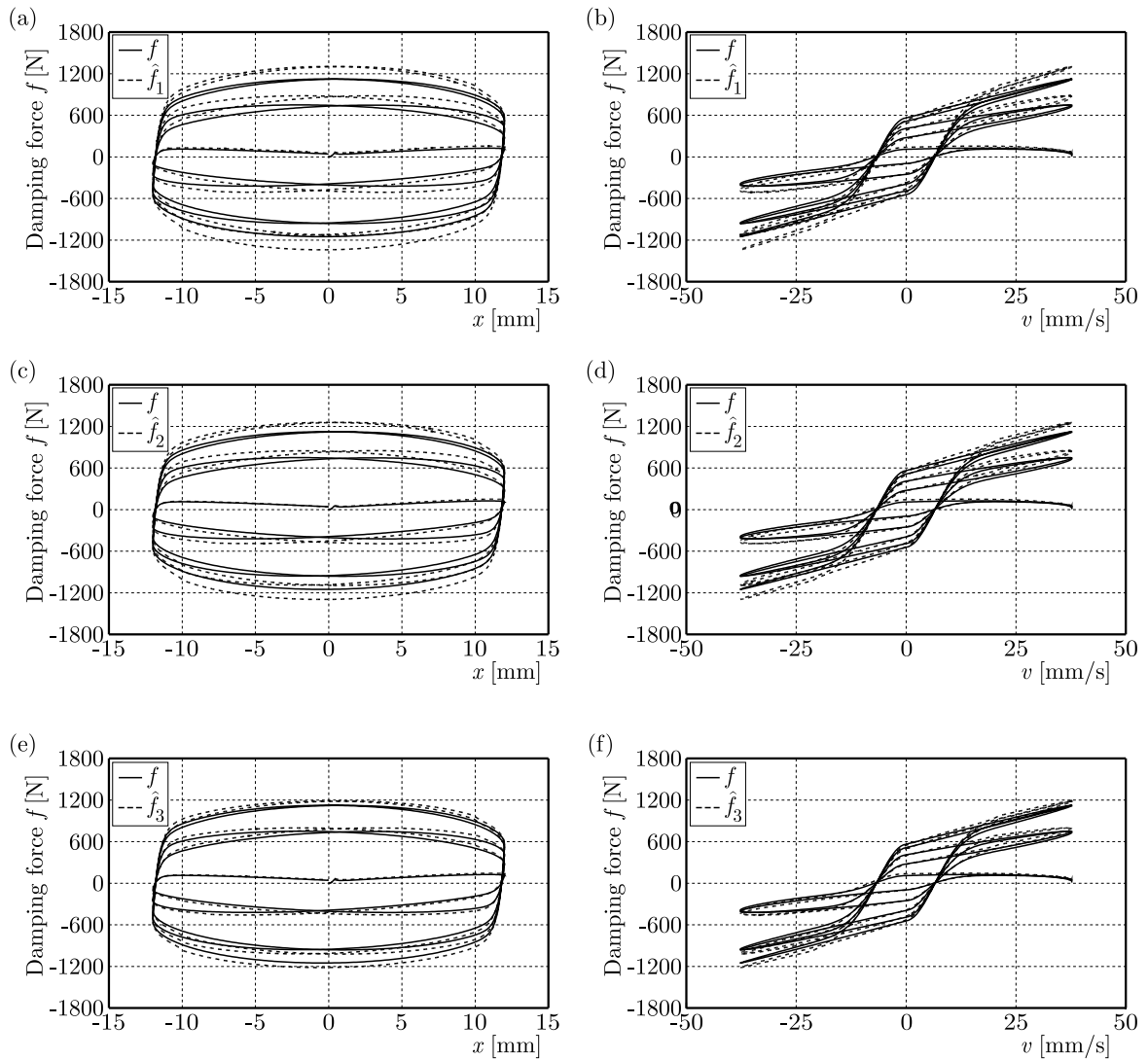


Fig. 7. Comparison of the response between f and $\hat{f}_{1,2,3}$

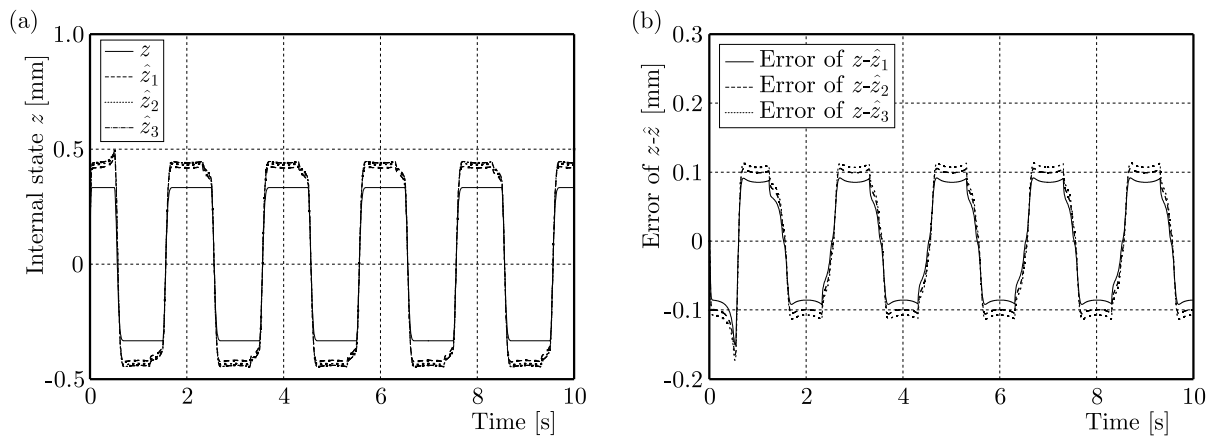


Fig. 8. Comparison of the responses between z and $\hat{z}_{1,2,3}$ by the SMO

of z and the estimated internal state of \hat{z} by the SMO is shown in Fig. 8. The real internal state of z is obtained from Eq. (2.1)₁ with the given value of $\alpha = 3$. The estimated internal states $\hat{z}_{1,3}$ are obtained by using the SMO with the identified values of $\hat{\alpha}$ in Table 2. It is revealed that the errors of z and \hat{z} are between 0.1 mm. It is also evident that the estimated state of \hat{z} is successfully estimated by using the SMO. Figure 9 displays a comparison between the real damping f and estimated damping forces $\hat{f}_{1,2,3}$. The error responses of $f - \hat{f}_{1,2,3}$ versus displacement and velocity are respectively shown in Figs. 9a and 9b. Here, it can be observed that the error responses of $f - \hat{f}_3$ are less than the other two errors. The error responses of $f - \hat{f}_{1,2,3}$ versus time are respectively shown in Figs. 9c and 9d, where it is evident that the error responses of $f - \hat{f}_{1,2,3}$ are also minimum.

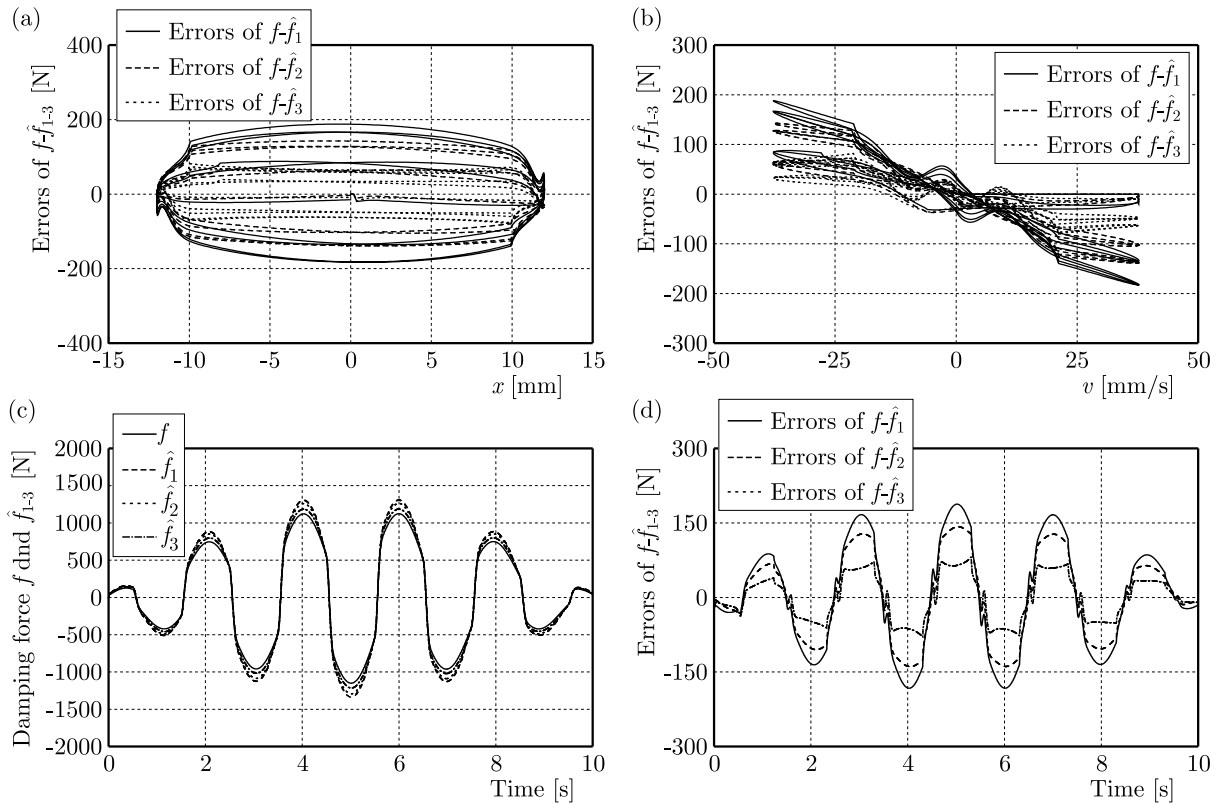


Fig. 9. Comparison of the responses between f and $\hat{f}_{1,2,3}$ by using the input voltage $U(t) = 10 \sin(\pi t/10)$ V

4.3. Discussion

In the numerical experiments, this paper proposes a methodology for parameter identification using the SLPSO for an MR damper with a new dynamic model. The real internal state, current and damping force are obtained from the dynamic model with given parameters and inputs. In practical conditions, the external excitation inputs (displacement and velocity) and input voltage are known, and the output is the exerted damping force. The parameters of the dynamic model are unknown. In this paper, three types of input voltages are implemented in the dynamic modeling. From the numerical experiments, three sets of parameters are revealed by three input voltages shown in Table 2. From a comparison of the response between the real damping force f and estimated damping forces $\hat{f}_{1,2,3}$, it is revealed that the estimated damping force \hat{f}_3 produced by the identified parameters is more similar to the real damping force f than the other two cases. Therefore, we can conclude that the responses found by using U_1 are dull,

and the responses by using U_2 are periodic, the two input voltages cannot excite the unknown parameters in the dynamic modelling. In contrast, the responses obtained by using U_3 are dynamic and varied, they can excite the unknown parameters by the SLPSO. Furthermore, the error responses between f and \hat{f}_3 are smaller than the other two error responses shown in Fig. 9. Therefore, the parameters identified by using U_3 are equivalent to the real parameters of the MR damper when the identification conditions (e.g., U , x , v and feasible domain) are known and bound. Finally, the proposed dynamic model for the MR damper is practical for use with the input voltage. The method of parameter identification for the MR damper by using the SMO and SLPSO is feasible and successfully applied in this study. The advantage of the proposed dynamic model with the input voltage is the ability of adjusting the MR damper force.

5. Conclusions

In the dynamic response of an MR damper, the relationship between the exerted damping force and the external excitation input velocity is termed the hysteresis phenomenon. It is interesting to formulate a dynamic model for the MR damper. Therefore, in this paper, we proposed a dynamic model based on the LuGre model and an electrical equation for the MR damper. Then, the damping force can be practically adjusted by using the input voltage. However, there are some unknown parameters in the dynamic model of the MR damper. Accordingly, parameter identification by using the SLPSO algorithm is proposed to identify these unknown parameters, and the SMO is used to estimate the unmeasurable states. From numerical experiments, it is clear that the unmeasurable states are correctly estimated by the proposed SMO. Then, the unknown parameters of the dynamic model have been successfully identified by the SLPSO algorithm. The contributions of this paper are as follows:

- a new dynamic model based on the LuGre model and an electrical equation for MR dampers is formulated to fit for the hysteresis behavior,
- for the proposed dynamic model, the damping force can be practically adjusted by using the input voltage,
- the SMO is proposed to estimate the unmeasurable states,
- the unknown parameters of the MR damper are successfully identified by using SLPSO algorithm.

In the future work, the proposed dynamic model of MR dampers can be integrated into suspension systems to perform semi-active vibration control.

References

1. AHMED K., YAN P., LI S., 2021, Duhem model-based hysteresis identification in piezo-actuated nano-stage using modified particle swarm optimization, *Micromachines*, **12**, 3, 315
2. AMBHORE N., HIVARALE S.D., PANGAVHANE D., 2013, A study of Bouc-Wen model of magnetorheological fluid damper for vibration control, *International Journal of Engineering Research and Technology (IJERT)*, **2**, 2, 1-6
3. ANDERSEN K.M., 2000, An elementary proof of Rayleigh's principle, *International Journal of Mathematical Education in Science and Technology*, **31**, 3, 449-453
4. BALAMURUGAN L., JANCIRANI J., 2013, Application of a new modified parametric algebraic model for magnetorheological damper in vehicle semi-active suspension, *International Journal of Automobile Engineering Research and Development*, **3**, 1, 1-14

5. BARTKOWSKI P., ZALEWSKI R., CHODKIEWICZ P., 2019, Parameter identification of Bouc-Wen model for vacuum packed particles based on genetic algorithm, *Archives of Civil and Mechanical Engineering*, **19**, 322-333
6. BHOWMIK S., 2011, *Modelling and Control of Magnetorheological Damper: Real-Time Implementation and Experimental Verification*, Department of Mechanical Engineering Technical University of Denmark
7. BOADA M.J.L., BOADA B.L., DIAZ V., 2018, A novel inverse dynamic model for a magnetorheological damper based on network inversion, *Journal of Vibration and Control*, **24**, 15, 3434-3453
8. GRACZYKOWSKI C., PAWŁOWSKI P., 2017, Exact physical model of magnetorheological damper, *Applied Mathematical Modelling*, **47**, 400-424
9. IKHOUANE F., RODELLAR J., 2005, On the hysteretic Bouc-Wen model, *Nonlinear Dynamics*, **42**, 63-78
10. IKHOUANE F., RODELLAR J., 2007, *Systems with Hysteresis: Analysis, Identification and Control Using the Bouc-Wen Model*, John Wiley & Sons
11. ISMAIL M., IKHOUANE F., RODELLAR J., 2009, The hysteresis Bouc-Wen model, a survey, *Archives of Computational Methods in Engineering*, **16**, 2, 161-188
12. JIMÉNEZ R., ÁLVAREZ-ICAIZA L., 2005, LuGre friction model for a magnetorheological damper, *Structural Control and Health Monitoring*, **12**, 91-116
13. LI C., YANG S., NGUYEN T.T., 2012, A self-learning particle swarm optimizer for global optimization problems, *IEEE Transactions on Systems, Man, and Cybernetics – Part B: Cybernetics*, **42**, 3, 627-646
14. METERED H., 2010, *Modelling and Control of Magnetorheological Dampers for Vehicle Suspension Systems*, School of Mechanical, Aerospace and Civil Engineering, University of Manchester
15. NAZ S., RAJA M.A.Z., MEHMOOD A., ZAMEER A., SHOAI B., 2021, Neuro-intelligent networks for Bouc-Wen hysteresis model for piezo stage actuator, *The European Physical Journal Plus*, **136**, 396
16. NGUYEN X.B., KOMATSUZAKI T., TRUONG H.T., 2022, Adaptive parameter identification of Bouc-Wen hysteresis model for a vibration system using magnetorheological elastomer, *International Journal of Mechanical Sciences*, **213**, 106848
17. NIOLA V., PALLI G., STRANO S., TERZO M., 2019, Nonlinear estimation of the Bouc-Wen model with parameter boundaries: Application to seismic isolators, *Computers and Structures*, **222**, 1-9
18. PELLICIARI M., MARANO G.C., CUOGHI T., BRISEGHIELLA B., LAVORATO D., TARANTINO A.M., 2018, Parameter identification of degrading and pinched hysteretic systems using a modified Bouc-Wen model, *Structure and Infrastructure Engineering*, **14**, 12, 1573-1585
19. PENG Y., YANG J., LI J., 2018, Parameter identification of modified Bouc-Wen model and analysis of size effect of magnetorheological dampers, *Journal of Intelligent Material Systems and Structures*, **29**, 7, 1464-1480
20. RAMLI M.H.M., MINH T.V., CHEN X., 2019, Pseudoextended Bouc-Wen model and adaptive control design with applications to smart actuators, *IEEE Transactions on Control Systems Technology*, **27**, 5, 2100-2109
21. ROUSSEL R., EDELEN A., RATNER D., DUBEY K., GONZALEZ-AGUILERA J.P., KIM Y.K., KUKLEV N., 2022a, Differentiable Preisach modeling for characterization and optimization of accelerator systems with hysteresis, *arXiv preprint*, arXiv:2202.07747
22. ROUSSEL R., EDELEN A., RATNER D., DUBEY K., GONZALEZ-AGUILERA J.P., KIM Y.K., KUKLEV N., 2022b, Differentiable Preisach modeling for characterization and optimization of particle accelerator systems with hysteresis, *Physical Review Letters*, **128**, 20, 204801

23. XU S., WU Z., WANG J., HONG K., HU K., 2022, Generalized regression neural network modeling based on inverse Duhem operator and adaptive sliding mode control for hysteresis in piezoelectric actuators, *Proceedings of the Institution of Mechanical Engineers, Part I: Journal of Systems and Control Engineering*, **236**, 5, 1029-1037
24. ZALEWSKI R., NACHMAN J., SHILLOR M., BAJKOWSKI J., 2014, Dynamic model for a magnetorheological damper, *Applied Mathematical Modelling*, **38**, 2366-2376
25. ZHAO X., WU S., PAN H., 2018, A hybrid model of magnetorheological dampers based on generalized hysteretic biviscous operators, *Journal of Intelligent Material Systems and Structures*, **29**, 14, 2979-2985
26. ZHU H., RUI X., YANG F., ZHU W., WEI M., 2019, An efficient parameters identification method of normalized Bouc-Wen model for MR damper, *Journal of Sound and Vibration*, **448**, 26, 146-158

Manuscript received November 20, 2022; accepted for print February 2, 2023